SIAM J. SCI. COMPUT.
Vol. 35, No. 2, pp. B315–B335

DYNAMIC ITERATION FOR COUPLED PROBLEMS OF ELECTRIC CIRCUITS AND DISTRIBUTED DEVICES*

ANDREAS BARTEL†, MARKUS BRUNK†, MICHAEL GÜNTHER†, AND SEBASTIAN SCHÖPS‡

Abstract. Coupled systems of differential-algebraic equations (DAEs) may suffer from instabilities during a dynamic iteration. We extend the existing analysis on recursion estimates, error propagation, and stability to (semiexplicit) index-1 DAEs. In this context, we discuss the influence of certain coupling structures and the computational sequence of the subsystems on the rate of convergence. Furthermore, we investigate in detail convergence and divergence for two coupled problems stemming from refined electric circuit simulation. These are the semiconductor-circuit and field-circuit couplings. We quantify the convergence rate and behavior also using Lipschitz constants and suggest an enhanced modeling of the coupling interface in order to improve convergence.

Key words. dynamic iteration, co-simulation, mixed mode simulation, partial differential-algebraic equations, coupling, electric circuit simulation

AMS subject classifications. 65L05, 65L80, 65L20

DOI. 10.1137/120867111

1. Introduction.

In today's applications, multiphysical modeling is indispensable due to miniaturization and the increasing complexity of components. Thus coupled simulation (or simulator coupling) is naturally needed. That is, different simulation packages are applied to different subsystems, and often one cannot solve the system as a whole in the time-domain. Even if this is possible, it remains a challenging task for time integrators: the intrinsic time rates of the subsystems can differ by several orders of magnitude and the structure of the subsystems can differ significantly, e.g., symmetry and definiteness of the system matrices. This holds in particular for applications from electrical engineering. When coupling an electric circuit to a distributed device (mixed mode simulation [15]), the circuit is commonly described by differential-algebraic equations (DAEs) using a network approach, whereas the device is modeled by partial differential equations (PDEs). The network system is typically not symmetric and typically integrated by direct solvers, whereas the discretized PDE typically forms a symmetric system that is commonly solved by iterative methods. Standard time integration is inefficient for those problems. One way to overcome this impasse is to revisit co-simulation [30].

This paper addresses the (time-domain) co-simulation of partial differential-algebraic equation (PDAE) systems, i.e., the time integration of systems of PDEs

*Submitted to the journal's Computational Methods in Science and Engineering section February 22, 2012; accepted for publication (in revised form) November 5, 2012; published electronically March 5, 2013. This work was supported by the ICESTARS project, which is funded by the Seventh Framework Programme of the European Union (grant ICT214911), and the SOFA project, funded by the BMBF (grant 03MS648E).

http://www.siam.org/journals/sisc/35-2/86711.html

†Applied Mathematics and Numerical Analysis, Bergische Universität Wuppertal, 42097 Wuppertal, Germany (bartel@math.uni-wuppertal.de, mail@markus-brunk.de, guenther@math.uni-wuppertal.de).

‡Graduate School CE, Technische Universität Darmstadt, Dolivostraße 15, 64293 Darmstadt, Germany (schoeps@gsc.tu-darmstadt.de). This author's work was supported by the "Excellence Initiative" of the German Federal and State Governments and the Graduate School of Computational Engineering at TU Darmstadt.

and DAEs by means of dynamic iteration. First, dynamic iteration has been applied to coupled ordinary differential equations (ODEs), where they are known to be unconditionally stable [22, 9]. Usually a windowing technique is applied to enhance convergence, i.e., the contractivity of the related fixed point operator. However, in the application of dynamic iteration schemes to DAEs, severe instabilities occurred. The contraction of the fixed point operator can be guaranteed only if a stability constraint is fulfilled. This concept dates back to Lelarasmee [19] and was applied for single window convergence [17, 6]. The error propagation for multiple windows has been analyzed for DAEs with a special coupling structure of Lagrangian type in [3]. In [12] the error transport was considered under the simplifying assumption that the DAE system can be reduced to its underlying ODE. The coupling structure and its influence on the stability of dynamic iteration was also studied in [18].

In this paper we present a generalization of previous work [3, 6] by extending their rigorous analysis. We deduce a similar contractivity condition, which ensures convergence of dynamic iteration schemes applied to index-1 DAEs that can be reformulated as a semiexplicit system. This includes, for example, all index-1 DAEs with constant mass matrices. By examination of the error propagation for the windowing technique, we prove that the dynamic iteration scheme is globally convergent if stability is given. We identify certain coupling structures where our analysis immediately guarantees a higher rate of convergence with respect to the time window size. This is of special interest for radio frequency applications, where the applied time window is usually rather small. We show that the sequence of computation of the subproblems can be crucial for convergence. Additionally, we verify that even if the iteration scheme is convergent independent of the sequence of the subsystems, the sequence can influence the rate of convergence. In applications from electrical engineering, the different coupling structures and their influence on convergence and the rate of convergence are investigated. For two different problems we suggest an enhanced modeling of the coupling interface (by overlapping or model parameter extraction) such that convergence is ensured and a higher rate of convergence can be achieved compared to coupling via the unmodified interface.

The paper is organized as follows. Following our introduction (section 1) we introduce in section 2 the notation for our coupled DAE-problems and the dynamic iteration schemes. In section 3 we analyze the convergence and stability of the dynamic iteration schemes. We consider the error transport for both differential and algebraic components and show that global convergence (including error transport) is ensured if the splitting error remains close to the analytical solution. Finally, we show that the mutual dependency of the subsystems, i.e., coupling via differential or algebraic variables, is crucial for the convergence of the iteration scheme. To apply the theoretical results in circuit simulation, we recall the electric network model and discuss coupling strategies in section 4. Based on this, we analyze two coupled problems. First, we investigate the semiconductor-circuit problem in section 5. Second, the field-circuit system is analyzed in section 6. In both applications, we focus on the modeling of the coupling interface: we show under which conditions the convergence behaves as in a coupled ODE problem and how this can be obtained by sophisticated modeling, e.g., overlapping or extraction of reduced models; cf. [12, 23]. Both examples numerically confirm the theoretical results about convergence and divergence. The conclusions from our analysis form the final section of this paper.

2. Description of coupled DAE systems for dynamic iteration schemes. We address the time domain simulation of coupled problems. To this end, we assume

that a suitable spatial discretization is already applied to a coupled PDAE problem and consider the time integration of the resulting coupled DAE problem. A large class of these initial value problems (IVPs) can be written in semiexplicit form:

$$\dot{\mathbf{y}} = \mathbf{f}(\mathbf{y}, \mathbf{z}), \qquad \mathbf{y}(0) = \mathbf{y}_0, \tag{2.1a}$$

$$0 = \mathbf{g}(\mathbf{y}, \mathbf{z}), \qquad \mathbf{z}(0) = \mathbf{z}_0. \tag{2.1b}$$

This formulation addresses the whole system at once but suppresses the subsystem structuring, which will serve to extract certain principal results and allow for condensed argumentations. Under the following assumption, $\mathbf{y}$ denotes the differential variables and $\mathbf{z}$ the algebraic variables of the system (2.1).

Assumption 2.1. Given problem (2.1), the following hold.

(a) The right-hand-side functions and the initial values (IVs) are assumed to guarantee a unique solution $\mathbf{x}$ on $[0, t_e]$:

$$\mathbf{x} := (\mathbf{y}, \mathbf{z})^\top \quad \text{with} \quad \mathbf{y} : [0, t_e] \to \mathbb{R}^{n_y},\ \mathbf{z} : [0, t_e] \to \mathbb{R}^{n_z}$$

(neglecting some transpose signs to keep the notation simple).

(b) Functions $\mathbf{f}$ and $\mathbf{g}$ are supposed to be sufficiently often differentiable in the neighborhood of the unique solution.

(c) The Jacobian $\partial \mathbf{g}/\partial \mathbf{z}$ is nonsingular in the neighborhood of the solution.

Assumption 2.1 ensures consistent IVs and that the system (2.1) is of index-1. In fact, system (2.1) can be easily generalized to larger classes, e.g., DAEs with constant (singular) mass matrices. However, the semiexplicit form allows a much simpler presentation.

2.1. Coupled system representation. In a multiphysical framework, system (2.1) is often naturally partitioned into a set of r coupled DAE subsystems:

$$\dot{\mathbf{y}}_i = \mathbf{f}_i(\mathbf{y}, \mathbf{z}), \qquad (\mathbf{y} = (\mathbf{y}_1, \ldots, \mathbf{y}_r)^\top), \tag{2.2a}$$

$$0 = \mathbf{g}_i(\mathbf{y}, \mathbf{z}), \qquad (\mathbf{z} = (\mathbf{z}_1, \ldots, \mathbf{z}_r)^\top) \tag{2.2b}$$

for $i = 1, \ldots, r$ and $\mathbf{f} = (\mathbf{f}_1, \ldots, \mathbf{f}_r)^\top$, $\mathbf{g} = (\mathbf{g}_1, \ldots, \mathbf{g}_r)^\top$. In order to ensure index-1 for each subsystem, in this framework, in addition to Assumption 2.1, it has to hold that

$$\partial \mathbf{g}_i/\partial \mathbf{z}_i \text{ is nonsingular for all } i = 1, \ldots, r; \tag{2.3}$$

i.e., each subsystem $\mathbf{g}_i(\mathbf{y}, \mathbf{z}) = 0$ is locally uniquely solvable for $\mathbf{z}_i$ (for given $\mathbf{y}$, $\mathbf{z}_1$, $\ldots$, $\mathbf{z}_{i-1}$, $\mathbf{z}_{i+1}$, $\ldots$, $\mathbf{z}_r$).

Remark 2.2 (overlapping). In some settings, certain quantities (and corresponding algebraic constraints) can be assigned to several subsystems. This is called *overlapping*. It introduces additional degrees of freedom to the latter dynamic iteration scheme; see, e.g., [4]. Here, these aspects are not discussed.

2.2. Iteration schemes. Given a general DAE (2.1), any dynamic iteration scheme needs to work on a split structure, e.g., on (2.2). This allows us to exploit particular properties by invoking dedicated solvers. To analyze dynamic iteration methods, we formalize this procedure. We seek to compute a sufficiently accurate numerical approximation $\tilde{\mathbf{x}}$ of the unique solution $\mathbf{x}$ for (2.1):

$$\tilde{\mathbf{x}} := (\tilde{\mathbf{y}}, \tilde{\mathbf{z}})^\top : [0, t_e] \to \mathbb{R}^{n_y} \times \mathbb{R}^{n_z}.$$

Usually the iteration is performed on so-called windows $[t_n, t_{n+1}]$ with $0 = t_0 < t_1 < t_2 < \cdots < t_N = t_e$ and window size $H_n := t_{n+1} - t_n$. Given a numerical approximation on $[0, t_n]$, a dynamic iteration defines the approximations on the subsequent window

$$(\tilde{\mathbf{y}}, \tilde{\mathbf{z}})|_{(t_n, t_{n+1}]} \in C_n^{1,0} \quad \text{with} \quad C_n^{1,0} := C^1\left((t_n, t_{n+1}], \mathbb{R}^{n_y}\right) \times C((t_n, t_{n+1}], \mathbb{R}^{n_z})$$

by an extrapolation step $\Phi_n : C_{n-1}^{1,0} \to C_n^{1,0}$ followed by k_n iterations $\Psi_n : C_n^{1,0} \to C_n^{1,0}$:

$$\begin{pmatrix} \tilde{\mathbf{y}}_n^{(0)} \\ \tilde{\mathbf{z}}_n^{(0)} \end{pmatrix} := \Phi_n \begin{pmatrix} \tilde{\mathbf{y}}|_{(t_{n-1}, t_n]} \\ \tilde{\mathbf{z}}|_{(t_{n-1}, t_n]} \end{pmatrix}, \quad \begin{pmatrix} \tilde{\mathbf{y}}_n^{(k-1)} \\ \tilde{\mathbf{z}}_n^{(k-1)} \end{pmatrix} \to \begin{pmatrix} \tilde{\mathbf{y}}_n^{(k)} \\ \tilde{\mathbf{z}}_n^{(k)} \end{pmatrix} := \Psi_n \begin{pmatrix} \tilde{\mathbf{y}}_n^{(k-1)} \\ \tilde{\mathbf{z}}_n^{(k-1)} \end{pmatrix}.$$

The simplest choice for Φ_n is constant extrapolation. The operator Ψ_n is the solution operator for the split version of the DAE problem (2.1):

$$\dot{\tilde{\mathbf{y}}}_n^{(k)} = \mathbf{F}(\tilde{\mathbf{y}}_n^{(k)}, \tilde{\mathbf{y}}_n^{(k-1)}, \tilde{\mathbf{z}}_n^{(k)}, \tilde{\mathbf{z}}_n^{(k-1)}) \quad \text{with IV} \quad \tilde{\mathbf{y}}_n^{(k)}(t_n) = \tilde{\mathbf{y}}_n^{(k-1)}(t_n), \tag{2.4a}$$

$$0 = \mathbf{G}(\tilde{\mathbf{y}}_n^{(k)}, \tilde{\mathbf{y}}_n^{(k-1)}, \tilde{\mathbf{z}}_n^{(k)}, \tilde{\mathbf{z}}_n^{(k-1)}). \tag{2.4b}$$

The $\mathbf{F}$ and $\mathbf{G}$ are arbitrary splitting functions, which are sufficiently differentiable, $\mathbf{G}_{\mathbf{z}^{(k)}}$ is regular and fulfills the compatibility conditions for problem (2.1):

$$\mathbf{F}(\mathbf{y}, \mathbf{y}, \mathbf{z}, \mathbf{z}) = \mathbf{f}(\mathbf{y}, \mathbf{z}), \qquad \mathbf{G}(\mathbf{y}, \mathbf{y}, \mathbf{z}, \mathbf{z}) = \mathbf{g}(\mathbf{y}, \mathbf{z}). \tag{2.5}$$

Thus the analytic solution $\mathbf{x} := (\mathbf{y}, \mathbf{z})^\top$ is a fixed point of the iteration operator Ψ_n.

Remark 2.3 (time discretization). Notice that in our dynamic iteration all DAE subsystems (2.2) are solved exactly; i.e., we disregard time-discretization errors. This is justified by the fact that for adequate time-steps the splitting error dominates.

In fact, for the partitioned system (2.2), the iteration operator Ψ_n splits into corresponding r IV problems. This is encoded by the splitting functions and use of new and old iterates for any dynamic iteration scheme. Common variants are Gauss–Seidel and Jacobi-type schemes; e.g., see [9].

Finally after extrapolation and k_n iterations, we obtain the approximation:

$$\begin{pmatrix} \tilde{\mathbf{y}}|_{(t_n, t_{n+1}]} \\ \tilde{\mathbf{z}}|_{(t_n, t_{n+1}]} \end{pmatrix} = (\Psi_n^{k_n} \circ \Phi_n)\left(\begin{pmatrix} \tilde{\mathbf{y}}|_{(t_{n-1}, t_n]} \\ \tilde{\mathbf{z}}|_{(t_{n-1}, t_n]} \end{pmatrix}\right).$$

Note that as a result of these assignments the algebraic variables $\tilde{\mathbf{z}}$ might not fulfill the constraints for the next time window (2.4b). Thus the overall numerical solution $\tilde{\mathbf{z}}$ might show discontinuities at time levels $t = T_n$, whereas $\tilde{\mathbf{y}}$ is continuous.

For coupled ODEs, the methods discussed above can be made convergent by choosing the window sizes sufficiently small. For DAEs an additional contractivity must be satisfied to obtain (a) the convergence of iterations within a window and (b) the stable error propagation in algebraic variables (window to window).

3. Analysis of convergence and stability. The convergence of dynamic iteration schemes is investigated by studying error recursions within one window and the error transport from window to window. We disregard errors from time integration; i.e., we iterate on analytically obtained waveforms. Our strategy generalizes the approach of [3] as already started in [6]. In the first part, we define the corresponding function space and deduce the error recursion on one window by tracking the constants in our estimates. Then, in the second part, we summarize the line of argument that guarantees contraction, general convergence, and stability. In the last part we investigate the implications of our results for the rate of convergence.

3.1. Error recursion on one window. We require that all numerical solutions remain in a neighborhood of the analytic solution. This is a well known requirement from DAE theory; cf. the convergence proof for backward differentiation formula methods, e.g., [16]. In our case this analysis has to be carried out in function space.

Given $d_0 > 0$, we define for all d with $0 < d \le d_0$ the function space $\mathcal{U}_{d,n}$ as neighborhood of the exact solution $\mathbf{x} := (\mathbf{y}, \mathbf{z})^\top$:

$$\mathcal{U}_{d,n} = \left\{ \mathbf{X} := (\mathbf{Y}, \mathbf{Z})^\top \in C_n^{1,0} : \left|\left|\mathbf{Y} - \mathbf{y}|_{(t_n, t_{n+1}]}\right|\right|, \left|\left|\mathbf{Z} - \mathbf{z}|_{(t_n, t_{n+1}]}\right|\right| \le d \right\}$$

on the nth window by employing $||\mathbf{v}|| := \sup_{t_n < t \le t_{n+1}} |\mathbf{v}(t)|$ and the Euclidean norm $|\cdot|$. The purpose of d_0 is to identify a largest function space $\mathcal{U}_{d_0,n}$ to be considered in the proofs below.

Assumption 3.1. For (2.1) with splitting functions $\mathbf{F}$, $\mathbf{G}$ there is $d_0 > 0$ with the following:

(3.1) $\mathbf{F}$ is Lipschitz-continuous on $\mathcal{U}_{d_0,n}$ with constant $L_{\mathbf{F}} > 0$.

(3.2) $\mathbf{G}$ is totally differentiable with Lipschitz-continuous derivatives on $\mathcal{U}_{d_0,n}$.

(3.3) $\mathbf{G}_{\mathbf{z}^{(k)}}$ (partial derivative) is nonsingular on $\mathcal{U}_{d_0,n}$.

Assumption 3.1 ensures that system (2.4) is index-1 with a well-defined solution. We prove contractivity in a smaller set $\mathcal{U}_{d,n} \subset \mathcal{U}_{d_0,n}$. For arbitrary $\mathbf{X}, \tilde{\mathbf{X}} \in \mathcal{U}_{d_0,n}$ and k dynamic iterations on the n-th time window, we introduce the abbreviations

$$(\mathbf{Y}_n^k, \mathbf{Z}_n^k)^\top := \Psi_n^k \mathbf{X}, \qquad (\tilde{\mathbf{Y}}_n^k, \tilde{\mathbf{Z}}_n^k)^\top := \Psi_n^k \tilde{\mathbf{X}}. \tag{3.4}$$

To measure the distance after k iterations, we define the notation

$$\begin{aligned} \Delta_{\mathbf{y}}^k(t) &:= \mathbf{Y}_n^k(t) - \tilde{\mathbf{Y}}_n^k(t), & \delta_{\mathbf{y}}^k &:= ||\Delta_{\mathbf{y}}^k|| = \sup_{t_n < t \le t_{n+1}} \left(\left|\Delta_{\mathbf{y}}^k(t)\right|\right), \\ \Delta_{\mathbf{z}}^k(t) &:= \mathbf{Z}_n^k(t) - \tilde{\mathbf{Z}}_n^k(t), & \delta_{\mathbf{z}}^k &:= ||\Delta_{\mathbf{z}}^k|| = \sup_{t_n < t \le t_{n+1}} \left(\left|\Delta_{\mathbf{z}}^k(t)\right|\right). \end{aligned} \tag{3.5}$$

For these errors, we have the following estimate.

LEMMA 3.2 (error recursion). *We consider the DAE* (2.1) *with a dynamic iteration* (2.4) *satisfying Assumptions* 2.1 *and* 3.1. *We assume having reached the nth window* $[t_n, t_{n+1}]$. *Then there are constants* $C, \tilde{c} > 1$, *such that for* $d < \min\{d_0/C,\ 1/(2\tilde{c})\}$ *and time step size* $H := t_{n+1} - t_n < H_0$ *the hypothesis* $\Psi_n^{k-1}\mathbf{X},\ \Psi_n^{k-1}\tilde{\mathbf{X}} \in \mathcal{U}_{d,n}$ *for* $k \ge 1$ *implies the recursion estimate*

$$\begin{pmatrix} \delta_{\mathbf{y}}^k \\ \delta_{\mathbf{z}}^k \end{pmatrix} \le \mathbf{K} \begin{pmatrix} \delta_{\mathbf{y}}^{k-1} \\ \delta_{\mathbf{z}}^{k-1} \end{pmatrix} + \begin{pmatrix} 1 + CH \\ C \end{pmatrix} |\Delta_{\mathbf{y}}^{k-1}(t_n)| \tag{3.6}$$

$$\textit{with} \qquad \mathbf{K} := \begin{pmatrix} CH & CH \\ C & CH + \alpha_n \end{pmatrix}, \qquad \alpha_n := (1 + \tilde{c}\, d) \left|\left| \mathbf{G}_{\mathbf{z}^{(k)}}^{-1}\, \mathbf{G}_{\mathbf{z}^{(k-1)}} \right|\right| + Cd. \tag{3.7}$$

In this statement $\Delta_{\mathbf{y}}^{k-1}(t_n) = \Delta_{\mathbf{y}}^0(t_n)$ is the difference between $\mathbf{X}(t_n)$ and $\tilde{\mathbf{X}}(t_n)$ and $||\cdot||$ denotes the supremum of the spectral norm on the nth window.

Proof. The proof has two parts corresponding to the two lines of the estimate (3.6). For the differential estimate, we write (2.4a) for both old iterates $\Psi_n^{k-1}\tilde{\mathbf{X}}$, $\Psi_n^{k-1}\mathbf{X}$. Integrating the difference, we obtain for the kth iterate (by Lipschitz continuity, consistency of $\mathbf{F}$)

$$|\Delta_{\mathbf{y}}^k(\tau)| \le |\Delta_{\mathbf{y}}^{k-1}(t_n)| + L_{\mathbf{F}} \int_{t_n}^{\tau} \left\{ |\Delta_{\mathbf{y}}^k| + |\Delta_{\mathbf{y}}^{k-1}| + |\Delta_{\mathbf{z}}^k| + |\Delta_{\mathbf{z}}^{k-1}| \right\} \mathrm{d}t. \tag{3.8}$$

Note that the solvability of the ODE (2.4a) is guaranteed by standard arguments for a sufficiently small $H := t_{n+1} - t_n < 1/C$ (where C is specified below).

By Assumption 3.1, we can solve (2.4b) for $\mathbf{Z}^{(k)} = \hat{\boldsymbol{\phi}}(\mathbf{Y}^{(k)}, \mathbf{Y}^{(k-1)}, \mathbf{Z}^{(k-1)})$. Lipschitz continuity of $\hat{\boldsymbol{\phi}}$ gives

$$|\Delta_{\mathbf{z}}^k| \;\le\; L_{\hat{\phi}} \left(|\Delta_{\mathbf{y}}^k| + |\Delta_{\mathbf{y}}^{k-1}| + |\Delta_{\mathbf{z}}^{k-1}|\right) \tag{3.9}$$

with constant $L_{\hat{\phi}} > 0$. Inserting this result into (3.8) and solving for $\delta_{\mathbf{y}}^k$ yield

$$\delta_{\mathbf{y}}^k \;\le\; \left(1 + \frac{L_0}{1 - L_0\, H}\, H\right) |\Delta_{\mathbf{y}}^{k-1}(t_n)| + \frac{L_0}{1 - L_0\, H}\, H \left(\delta_{\mathbf{y}}^{k-1} + \delta_{\mathbf{z}}^{k-1}\right) \tag{3.10}$$

with $L_0 := L_{\mathbf{F}}(1 + L_{\hat{\phi}})$. For $H < H_0 := 1/(2L_0)$ we have $L_0\, H < 1/2$ and it holds that

$$\delta_{\mathbf{y}}^k \;\le (1 + 2L_0 H)\, |\Delta_{\mathbf{y}}^{k-1}(t_n)| + 2L_0 H \big(\delta_{\mathbf{y}}^{k-1} + \delta_{\mathbf{z}}^{k-1}\big). \tag{3.11}$$

This is the first line of estimate (3.6) for a sufficiently large constant C; see below. Using estimates (3.9) and (3.11) twice for the two particular choices (a) $\mathbf{X} = \mathbf{x}|_{[t_n, t_{n+1}]}$ and $\tilde{\mathbf{X}}$ arbitrary and (b) $\mathbf{X}$ arbitrary and $\tilde{\mathbf{X}} = \mathbf{x}|_{[t_n, t_{n+1}]}$, one obtains from $\mathbf{X}_n^{k-1}, \tilde{\mathbf{X}}_n^{k-1} \in \mathcal{U}_{d,n}$ on $[t_n,\, t_{n+1}]$

$$\big|\big|\mathbf{Y}_n^k - \mathbf{y}\big|\big|,\, \big|\big|\tilde{\mathbf{Y}}_n^k - \mathbf{y}\big|\big| \le 4d, \qquad \big|\big|\mathbf{Z}_n^k - \mathbf{z}\big|\big|,\, \big|\big|\tilde{\mathbf{Z}}_n^k - \mathbf{z}\big|\big| \le 6L_{\hat{\phi}}\, d. \tag{3.12}$$

Thus $\mathbf{X}_n^k, \tilde{\mathbf{X}}_n^k \in \mathcal{U}_{d_0,n}$ for a sufficiently large constant $C > \max\{2L_0,\, 4,\, 6L_{\hat{\phi}}\}$.

Second, we establish the algebraic part of (3.6) by a homotopy; for $\theta \in [0, 1]$ let

$$\mathbf{Y}^{(k),\theta}(t) := \theta \tilde{\mathbf{Y}}_n^k(t) + (1-\theta)\mathbf{Y}_n^k(t) \quad \text{and} \quad \mathbf{Z}^{(k),\theta}(t) := \theta \tilde{\mathbf{Z}}_n^k(t) + (1-\theta)\mathbf{Z}_n^k(t).$$

We use the abbreviation (with $\mathbf{u}$ denoting an arbitrary argument of $\mathbf{G}$)

$$\mathbf{G}(\theta) := \mathbf{G}\big(\mathbf{Y}^{(k),\theta},\, \mathbf{Y}^{(k-1),\theta},\, \mathbf{Z}^{(k),\theta},\, \mathbf{Z}^{(k-1),\theta}\big) \qquad \text{and} \qquad \mathbf{G}_{\mathbf{u}}(\theta) := \frac{\partial \mathbf{G}}{\partial \mathbf{u}}(\theta).$$

Thus it holds that $\mathbf{G}(0) = \mathbf{G}(1) = 0$ and therefore

$$\begin{aligned} 0 = \mathbf{G}(1) - \mathbf{G}(0) = \int_0^1 \Big(& \mathbf{G}_{\mathbf{y}^{(k)}}(\theta)\Delta_{\mathbf{y}}^k + \mathbf{G}_{\mathbf{y}^{(k-1)}}(\theta)\Delta_{\mathbf{y}}^{k-1} \\ & + \mathbf{G}_{\mathbf{z}^{(k)}}(\theta)\, \Delta_{\mathbf{z}}^k + \mathbf{G}_{\mathbf{z}^{(k-1)}}(\theta)\, \Delta_{\mathbf{z}}^{k-1} \Big) \mathrm{d}\theta. \end{aligned} \tag{3.13}$$

Employing $\frac{\partial}{\partial\theta}\mathbf{Y}^{(k),\theta} = \Delta_{\mathbf{y}}^k$, etc., Lipschitz continuity of $\mathbf{G}_{\mathbf{z}^{(k)}}$ on $\mathcal{U}_{d_0,n}$ for $Cd \le d_0$ with constant $L_{\mathbf{G}'}$, and estimate (3.12), we obtain for any time $t \in [t_n, t_{n+1}]$

$$\begin{aligned} |\mathbf{G}_{\mathbf{u}}(\theta) - \mathbf{G}_{\mathbf{u}}(0)| &\le L_{\mathbf{G}'} \Big(\big|\theta\tilde{\mathbf{Y}}_n^k(t) + (1-\theta)\mathbf{Y}_n^k(t) - \mathbf{Y}_n^k(t)\big| + \cdots \\ &\qquad + \big|\theta\tilde{\mathbf{Z}}_n^{k-1}(t) + (1-\theta)\mathbf{Z}_n^{k-1}(t) - \mathbf{Z}_n^{k-1}(t)\big| \Big) \\ &= L_{\mathbf{G}'}\theta \Big(|\Delta_{\mathbf{y}}^k| + |\Delta_{\mathbf{y}}^{k-1}| + |\Delta_{\mathbf{z}}^k| + |\Delta_{\mathbf{z}}^{k-1}| \Big) \le 12(1 + L_{\hat{\phi}}) L_{\mathbf{G}'} d. \end{aligned} \tag{3.14}$$

By Assumption 3.1 $\mathbf{G}_{\mathbf{z}^{(k)}}(0)$ is regular, so from estimate (3.13) we obtain

$$\begin{aligned} 0 = \int_0^1 \mathbf{G}_{\mathbf{z}^{(k)}}^{-1}(0) \Big(& \mathbf{G}_{\mathbf{y}^{(k)}}(\theta)\Delta_{\mathbf{y}}^k + \mathbf{G}_{\mathbf{y}^{(k-1)}}(\theta)\Delta_{\mathbf{y}}^{k-1} + \big(\mathbf{G}_{\mathbf{z}^{(k)}}(0) + \big[\mathbf{G}_{\mathbf{z}^{(k)}}(\theta) - \mathbf{G}_{\mathbf{z}^{(k)}}(0)\big]\big)\Delta_{\mathbf{z}}^k \\ & + \big(\mathbf{G}_{\mathbf{z}^{(k-1)}}(0) + \big[\mathbf{G}_{\mathbf{z}^{(k-1)}}(\theta) - \mathbf{G}_{\mathbf{z}^{(k-1)}}(0)\big]\big)\Delta_{\mathbf{z}}^{k-1} \Big)\, \mathrm{d}\theta. \end{aligned}$$

Due to our smoothness assumptions, all operators $\mathbf{G}^{-1}_{\mathbf{z}^{(k)}}$, $\mathbf{G}_{\mathbf{z}^{(k-1)}}$, $\mathbf{G}_{\mathbf{y}^{(k)}}$, $\mathbf{G}_{\mathbf{y}^{(k-1)}}$ are uniformly bounded on $\mathcal{U}_{d_0,n}$ with a constant c_g. Solving the last equation for

$$\mathbf{G}^{-1}_{\mathbf{z}^{(k)}}(0)\mathbf{G}_{\mathbf{z}^{(k)}}(0)\Delta^k_{\mathbf{z}} = \Delta^k_{\mathbf{z}},$$

we obtain for the maximum norm when using (3.14)

$$\delta^k_{\mathbf{z}} \le \Big(||\mathbf{G}^{-1}_{\mathbf{z}^{(k)}}\,\mathbf{G}_{\mathbf{z}^{(k-1)}}|| + \frac{\tilde{c}}{2}d\Big)\,\delta^{k-1}_{\mathbf{z}} \;+\; \frac{\tilde{c}}{2}\,d\,\delta^k_{\mathbf{z}} \;+\; c_g^2\,\big(\delta^k_{\mathbf{y}} + \delta^{k-1}_{\mathbf{y}}\big),$$

where $\tilde{c} := 24(1 + L_{\hat{\phi}})L_{\mathbf{G}'}c_g$ and

$$||\mathbf{G}^{-1}_{\mathbf{z}^{(k)}}\mathbf{G}_{\mathbf{z}^{(k-1)}}|| = ||\mathbf{G}^{-1}_{\mathbf{z}^{(k)}}\mathbf{G}_{\mathbf{z}^{(k-1)}}||(0) = \big|\big|\mathbf{G}^{-1}_{\mathbf{z}^{(k)}}\mathbf{G}_{\mathbf{z}^{(k-1)}}\big|\big|\big(\mathbf{Y}^k_n(t), \mathbf{Y}^k_n(t), \mathbf{Z}^k_n(t), \mathbf{Z}^k_n(t)\big).$$

Last, we use the estimate (3.11) for $\delta^k_{\mathbf{y}}$. For $H < 1/C$ and $d < \frac{1}{2\tilde{c}}$, we find

$$\begin{aligned}\delta^k_{\mathbf{z}} &\le 3(1+\tilde{c}d)c_g^2\Big(|\Delta^{k-1}_{\mathbf{y}}(t_n)| + \delta^{k-1}_{\mathbf{y}}\Big)\\ &\quad + (1+\tilde{c}d)\Big(2c_g^2L_0H + ||\mathbf{G}^{-1}_{\mathbf{z}^{(k)}}\,\mathbf{G}_{\mathbf{z}^{(k-1)}}|| + \frac{\tilde{c}}{2}d\Big)\,\delta^{k-1}_{\mathbf{z}}.\end{aligned} \tag{3.15}$$

The global constant C must be large enough to deduce the self-mapping (3.12) and to deduce the error recursion claim (3.6) from estimates (3.11) and (3.15); this gives

$$C > \max\left\{2L_0,\ 4,\ 6L_{\hat{\phi}},\ 3(1+\tilde{c}d_0)c_g^2, (1+\tilde{c}d_0)c_g^2L_0, \frac{\tilde{c}}{2}\right\}$$

with $d < d_0$. ∎

This estimate is used to verify that the mapping defined by our dynamic iteration scheme is a fixed point operator. In contrast to related works, the origins of the constants in the proof remain visible. This will be exploited in the later applications to achieve a better rate of convergence by enhanced modeling of the coupling interface. However, the structure of the estimate is similar in the known literature [3]. Since $|\Delta^{k-1}_{\mathbf{y}}(t_n)| \le \delta^{k-1}_{\mathbf{y}}$, one has some freedom in stating (3.6), e.g., ignoring then the special role of the initial values.

3.2. Convergence and stability. Based on the error recursion estimate (3.6), we can follow the line of [3] to investigate convergence and stability for our generalized setting (2.1). According to (3.6) the spectral radius of the iteration matrix must satisfy $\rho(\mathbf{K}) < 1$ to establish contractivity. Inspecting the eigenvalues

$$\lambda_{1,2}(\mathbf{K}) = \frac{1}{2}\Big(\alpha_n + 2\,CH \pm \sqrt{\alpha_n^2 + 4\,C^2H}\Big), \tag{3.16}$$

we find that $\alpha_n < 1$ is sufficient for contraction (given H small enough).

THEOREM 3.3 (contraction). *Given an index-1 DAE (2.1) (Assumption 2.1) with splitting functions fulfilling Assumption 3.1 and an extrapolation operator with accuracy $\mathcal{O}(H)$, and given $d < d_0$ and $H < H_0$ small enough,*

$$\big|\big|\mathbf{G}^{-1}_{\mathbf{z}^{(k)}}\,\mathbf{G}_{\mathbf{z}^{(k-1)}}\big|\big| < 1 \tag{3.17}$$

implies that the local error decreases with each iteration (Ψ is strongly contractive).

Notice that (3.17) implies indeed $\alpha_n < 1$ in (3.7) for d and H small enough and therefore it implies contraction. Thus, it follows from Theorem 3.3 that the local splitting error can be made arbitrarily small as $k \to \infty$.

Employing a similar estimation for the propagated error, one finally obtains stability. The key is to ensure, additionally to Theorem 3.3,

$$\alpha_n \le \alpha < 1 \qquad \text{and} \qquad L_\Phi \alpha_n^{k_n} \le \alpha.$$

Then it can be shown that the global error is bounded. Detailed arguments are found, for example, in [3].

3.3. Rate of convergence. We have seen that $\rho(\mathbf{K})$ governs (the speed of) convergence. As the rate of convergence of the dynamic iteration (2.4), we inspect the asymptotics of $\rho(\mathbf{K})$ as $H \to 0$ for different coupling structures, which then leads to a corollary for Theorem 3.3. Finally, we will identify former results from literature as special cases of our generalized approach.

Remark 3.4 (convergence rate of fixed point iteration).

(i) For $\alpha_n \neq 0$, a Taylor expansion of the square root in $\lambda(\mathbf{K})$ (3.16) yields (for the expansion point $H = 0$)

$$\sqrt{\alpha_n^2 + 4\,C^2 H} = \alpha_n\,(1 + 2\,C^2 H/\alpha_n^2) + \mathcal{O}(H^2).$$

Thus, if $4\,C^2 H < \alpha_n^2$ (we can indeed disregard higher order terms), then the rate is $\alpha_n + \mathcal{O}(H)$.

(ii) The convergence of the distributed DAE-time integration also requires the stability of the coupling of old with new algebraic components (3.17).
The computational sequence of the subsystems is reflected in the splitting functions; thus (3.17) may change for different sequences, e.g., when using a Gauss–Seidel scheme (see section 5.4 for an example).

If possible, the time integration of coupled DAEs should be performed such that contraction is directly ensured, such as in the following special cases. Here contraction is guaranteed by inspecting the structure of the coupling (cf. [6]). The results are obtained by following the lines of the proof of Lemma 3.2 but exploiting the particular structure.

COROLLARY 3.5 (simple coupling). *We assume the hypothesis of Lemma* 3.2.

(i) *For a splitting, where no algebraic constraint relies on old algebraic iterates, i.e.,*

$$\mathbf{G}_{\mathbf{z}^{(k-1)}} = 0, \tag{3.18}$$

a recursion estimate of the form (3.6) *can then be proven where* $\alpha_n = 0$. *Contraction follows with rate* $\mathcal{O}(\sqrt{H})$.

(ii) *Given a splitting where no algebraic constraint depends on old iterates, i.e.,*

$$\mathbf{G}_{\mathbf{z}^{(k-1)}} = 0 \quad \textit{and} \quad \mathbf{G}_{\mathbf{y}^{(k-1)}} = 0, \tag{3.19}$$

contraction follows with rate $\mathcal{O}(H)$.

Remark 3.6 (fractional step). Corollary 3.5(i) includes the special case of a Gauss–Seidel-type iteration scheme for a semiexplicit DAE (index-1), where one subsystem is the ODE and the other subsystem is the algebraic equation, i.e.,

$$\mathbf{F} := \mathbf{f}(\mathbf{y}^{(k)}, \mathbf{z}^{(k-1)}) \quad \text{and} \quad \mathbf{G} := \mathbf{g}(\mathbf{y}^{(k)}, \mathbf{z}^{(k)}). \tag{3.20}$$

For this so-called fractional step method applied to index-1 DAEs, the convergence rate $\mathcal{O}(H)$ has been proven independently [29].

4. Applications in electric circuit simulation. In circuit simulation, e.g. [10], electromagnetic devices and semiconductor devices are modeled as a network of idealized basic elements (resistors, inductors, capacitors and sources). The network approach yields a system of DAEs, such that the entire circuit can be simulated using common circuit simulation tools. However, many devices cannot be given sufficiently accurately in terms of idealized lumped elements. This requires the hierarchical coupling of PDE device models to the network. Space-discretization turns this into a DAE-DAE coupled problem.

The common monolithic simulation is often cumbersome or sometimes even impossible due to incompatible simulation tools. For example, a circuit simulator and a device simulator may not have interfaces to interchange all necessary data during transient simulations. On the other hand, the injection of lumped parameters, i.e., currents, into the circuit simulator is not a problem. This will be exploited by the co-simulation scheme given below.

4.1. Electric circuit model. Circuit simulators are commonly based on the flux/charge oriented modified nodal analysis (MNA) (see, e.g., [14]):

$$\mathbf{A}_{\mathrm{C}}\frac{\mathrm{d}}{\mathrm{d}t}\mathbf{q} + \mathbf{A}_{\mathrm{R}}\mathbf{g}_{\mathrm{R}}(\mathbf{A}_{\mathrm{R}}^{\top}\mathbf{u}, t) + \mathbf{A}_{\mathrm{L}}\mathbf{i}_{\mathrm{L}} + \mathbf{A}_{\mathrm{V}}\mathbf{i}_{\mathrm{V}} + \mathbf{A}_{\mathrm{I}}\mathbf{i}(t) + \mathbf{A}_{\mathrm{D}}\mathbf{i}_{\mathrm{D}} = \mathbf{0}, \tag{4.1a}$$

$$\frac{\mathrm{d}}{\mathrm{d}t}\mathbf{\Phi} - \mathbf{A}_{\mathrm{L}}^{\top}\mathbf{u} = \mathbf{0}, \qquad \mathbf{A}_{\mathrm{V}}^{\top}\mathbf{u} - \mathbf{v}(t) = \mathbf{0}, \tag{4.1b}$$

$$\mathbf{q} - \mathbf{q}_{\mathrm{C}}(\mathbf{A}_{\mathrm{C}}^{\top}\mathbf{u}, t) = \mathbf{0}, \qquad \mathbf{\Phi} - \mathbf{\Phi}_{\mathrm{L}}(\mathbf{i}_{\mathrm{L}}, t) = \mathbf{0}, \tag{4.1c}$$

where $\mathbf{q}_{\mathrm{C}}(\mathbf{v}, t)$, $\mathbf{g}_{\mathrm{R}}(\mathbf{v}, t)$, $\mathbf{\Phi}_{\mathrm{L}}(\mathbf{i}, t)$, $\mathbf{v}_{\mathrm{S}}(t)$, and $\mathbf{i}_{\mathrm{S}}(t)$ denote the element contributions as charges, currents of resistors, fluxes, voltage, and current sources, respectively. The matrices $\mathbf{A}_{\star}$ denote network incidences, and finally $\mathbf{i}_{\mathrm{D}}$ is the current injected from the semiconductor or field device (simulator), as discussed below. The unknowns of the circuit model equations are charges $\mathbf{q}(t)$, fluxes $\mathbf{\Phi}(t)$, currents $\mathbf{i}_{\mathrm{L}}(t)$, $\mathbf{i}_{\mathrm{V}}(t)$ through inductors and voltage sources, as well as all node potentials $\mathbf{u}(t)$ except ground.

In the following, we assume the standard conditions, such that the circuit equations (4.1) are of index-1 for a given function $\mathbf{i}_{\mathrm{D}}(t)$: namely, locally positive definite element contributions, and there is neither a CV-loop nor an LI-cutset [13].

4.2. Coupling settings. Next, we consider a circuit coupled to two different devices of very different scale: in section 5 the semiconductor-circuit coupling, where we use a one-dimensional (1D) PDE model of a *pn*-diode, and in section 6 the field-circuit coupling, where we employ a two-dimensional (2D) model of a transformer. In both cases, different coupling techniques and interfaces are discussed: (A) source coupling and (B) coupling using extracted, lumped parameters. The source coupling approach represents a black-box coupling where the circuit does not see the physics of the device. The lumped parameter approach, on the other hand, includes further physical effects. It fits into the framework of [12], where compact models are used as predictors in the coupled simulation. Moreover, it is related to the DIRM approach: dynamic iteration using reduced order models [23].

Furthermore, we will show that the sequence of solving the subsystems can be crucial for convergence of the iteration. Thus we discuss (i) device-first and (ii) circuit-first. Finally, we investigate the convergence rate of the fixed point iteration in terms of the time window size in the cases mentioned.

5. Semiconductor-circuit coupling. First we state the drift-diffusion model (spatially discretized). Then we discuss the two types of circuit coupling.

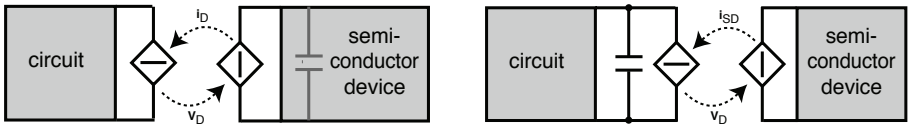

(a) Source coupling. (b) Coupling with capacitance.

FIGURE 5.1. *Displacement current modeled inside the PDE device* (a) *and by capacitance extraction in circuit* (b)*; see* [2].

5.1. Semiconductor model. The *pn*-diode in our example is described by the domain $\Omega \subset \mathbb{R}^d$ for $d = 1, 2, 3$ with $\partial\Omega = \Gamma = \Gamma_D \cup \Gamma_N$. Its physical behavior is modeled by the drift-diffusion (DD) model, which consists of conservation laws for the electron and hole densities coupled to the Poisson equation for the electric potential [27]. To ensure nonnegativity of the carrier densities, the DD-equations are discretized using exponentially fitted mixed finite elements as described in [20, 8]. Thus the discretized DD-equations read as

$$\mathbf{A}_\mathrm{n}(\mathbf{V})\frac{\mathrm{d}}{\mathrm{d}t}\mathbf{n} + \mathbf{B}_\mathrm{n}(\mathbf{p},\mathbf{V})\mathbf{n} = \mathbf{f}_\mathrm{n}(\mathbf{p},\mathbf{V}), \quad \mathbf{A}_\mathrm{p}(\mathbf{V})\frac{\mathrm{d}}{\mathrm{d}t}\mathbf{p} + \mathbf{B}_\mathrm{p}(\mathbf{n},\mathbf{V})\mathbf{p} = \mathbf{f}_\mathrm{p}(\mathbf{n},\mathbf{V}), \tag{5.1a}$$

$$\mathbf{L}\mathbf{V} = \mathbf{n} - \mathbf{p} - \mathbf{C} + \mathbf{f}_\mathrm{V}(\mathbf{v}_\mathrm{D}), \tag{5.1b}$$

$$\mathbf{i}_\mathrm{D} = \mathrm{j}_\mathrm{D}(\mathbf{n},\mathbf{p},\mathbf{V}), \tag{5.1c}$$

with nonsingular matrices $\mathbf{A}_\mathrm{n}, \mathbf{A}_\mathrm{p}, \mathbf{B}_\mathrm{n}, \mathbf{B}_\mathrm{p}, \mathbf{L}$ (cf. [8, 2]). Here $\mathbf{n}, \mathbf{p}, \mathbf{C}$, and $\mathbf{V}$ denote the discrete approximations of the electron and hole density, the doping profile, and the potential. The applied voltage drop is given by $\mathbf{v}_\mathrm{D}$. The total current $\mathbf{i}_\mathrm{D}$ leaving the device takes into account the particle current as well as the displacement current. The boundary conditions employed for the system are incorporated in the functions $\mathbf{f}_\mathrm{n}, \mathbf{f}_\mathrm{p}$, and $\mathbf{f}_\mathrm{V}$; for details we refer to [2]. We note that standard finite element or finite difference discretization would allow for a similar representation.

Alternatively the displacement current can be expressed in terms of a capacitance C_D and the time derivative of the applied voltage drop [1]. Instead of (5.1c) the total current can be written as

$$\mathbf{i}_\mathrm{D} = C_\mathrm{D}\frac{\mathrm{d}}{\mathrm{d}t}\mathbf{v}_\mathrm{D} - \mathbf{i}_\mathrm{SD} \quad \text{with} \quad \mathbf{i}_\mathrm{SD} := j_\mathrm{SD}(\mathbf{n},\mathbf{p},\mathbf{V}). \tag{5.1d}$$

In the case of a 1D model for a cubic diode with length l and cross-section A, it holds that $C_\mathrm{D} = \epsilon_s \cdot A/l$, where ϵ_s denotes the material's permittivity.

5.2. Coupling types. The structure of the equations allows for two different representations: (a) coupling by plain sources (*source coupling*), in which the displacement current is considered as part of the distributed device model, i.e., $\mathbf{i}_\mathrm{D}$ is defined by (5.1c), and (b) coupling where the displacement current is described in terms of circuit variables, i.e., (5.1d) is treated as an additional circuit equation (*coupling with capacitance*); see Figure 5.1. In both settings the voltage drop $\mathbf{v}_\mathrm{D}$ in the circuit describes the boundary condition for the electric potential $\mathbf{V}$ in the device model. In the case of a monolithic coupling, those two representations are equivalent, but in the case of a weak coupling by a dynamic iteration scheme, they exhibit different behavior. Since the additional capacity C_D in the circuit model (in setting (b)) can be considered as a simple compact model for the capacitive behavior of the diode, the *coupling with capacitances* reflects compact model design.

(a) Source coupling. For given $\mathbf{v}_\mathrm{D}$ the spatial discretization of the DD-equations (5.1) yields an index-1 DAE [8]. Moreover, we assume the coupled system to be of

index-1 [26]; i.e., no additional CV-loop is introduced by the coupling. Then the system can be written in semiexplicit form (d for device and c for circuit):

$$\begin{aligned} \dot{\mathbf{y}}_d &= \mathbf{f}_d(\mathbf{y}_d, \mathbf{z}_d), & \dot{\mathbf{y}}_c &= \mathbf{f}_c(\mathbf{y}_c, \mathbf{z}_c, \mathbf{z}_d), \\ \mathbf{0} &= \mathbf{g}_d(\mathbf{y}_d, \mathbf{z}_d, \mathbf{z}_c), & \mathbf{0} &= \mathbf{g}_c(\mathbf{y}_c, \mathbf{z}_c, \mathbf{z}_d), \end{aligned} \tag{5.2}$$

with nonsingular $\partial \mathbf{g}_d/\partial \mathbf{z}_d$ and $\partial \mathbf{g}_c/\partial \mathbf{z}_c$. The differential variables of the diode and circuit are $\mathbf{y}_d := (\mathbf{n}, \mathbf{p})$ and $\mathbf{y}_c := (\mathbf{q}, \mathbf{\Phi})$, whereas the corresponding algebraic unknowns are $\mathbf{z}_d = (\mathbf{V}, \mathbf{i}_\mathrm{D})$ and $\mathbf{z}_c := (\mathbf{u}, \mathbf{i}_\mathrm{L}, \mathbf{i}_\mathrm{V})$. Here the device current $\mathbf{i}_\mathrm{D}$ is defined by (5.1c).

In fact, the spatial discretization by the positivity-preserving mixed finite element scheme might turn some components of $\mathbf{n}, \mathbf{p}$ into algebraic variables [8]. However, this would not affect our iteration scheme as long as the index-1 assumptions hold.

In this setting all node potentials $\mathbf{u}$ and thus $\mathbf{v}_\mathrm{D} = \mathbf{A}_\mathrm{D}^\top \mathbf{u}$ are algebraic variables of the circuit. Thus the algebraic equations of the device $\mathbf{0} = \mathbf{g}_d$ depend only on the algebraic variable $\mathbf{z}_c$ of the circuit. The diode current is also algebraic, but, depending on the circuit's topology, it may appear in the differential $\mathbf{f}_c$ as well as in the algebraic equation $\mathbf{g}_c$ of system (5.2).

(b) Coupling with capacitance. Now we use the definition of $\mathbf{i}_\mathrm{D}$ from (5.1d) in the current balance equation (4.1a). This leads to a slightly different system:

$$\begin{aligned} \dot{\mathbf{y}}_d &= \mathbf{f}_d(\mathbf{y}_d, \mathbf{z}_d), & \dot{\mathbf{y}}_c &= \mathbf{f}_c(\mathbf{y}_c, \mathbf{z}_c, \mathbf{z}_d), \\ \mathbf{0} &= \mathbf{g}_d(\mathbf{y}_d, \mathbf{z}_d, \mathbf{y}_c), & \mathbf{0} &= \mathbf{g}_c(\mathbf{y}_c, \mathbf{z}_c), \end{aligned} \tag{5.3}$$

with differential unknowns $\mathbf{y}_d := (\mathbf{n}, \mathbf{p})$ and $\mathbf{y}_c := (\mathbf{q}, \mathbf{\Phi}, \mathbf{P}_D \mathbf{u})$ and algebraic unknowns $\mathbf{z}_d = (\mathbf{V}, \mathbf{i}_\mathrm{SD})$ and $\mathbf{z}_c := (\mathbf{Q}_D \mathbf{u}, \mathbf{i}_\mathrm{L}, \mathbf{i}_\mathrm{V})$. Here $\mathbf{Q}_D$ denotes a projector onto the kernel of $\mathbf{A}_\mathrm{D}^\top$ and $\mathbf{P}_D$ its complement, as they typically appear in circuit index analysis [13]. In this formulation the node potentials are split, since the capacitance C_D is not written in charge oriented form. Due to the linearity of C_D the advantage of the charge/flux oriented MNA, i.e., charge conservation, is still respected.

As a result of the capacitive path between the coupling nodes, $\mathbf{v}_\mathrm{D}$ is part of the differential variables $\mathbf{y}_c$ and the algebraic equations of the device subsystem only depend on differential circuit variables. In turn, the device current $\mathbf{i}_\mathrm{SD}$—an algebraic device variable—enters differential equations $\mathbf{f}_c$ of the circuit subsystem only.

5.3. Dynamic iteration for the semiconductor-circuit system. Based on the theory stated above, we discuss the convergence properties of the dynamic iteration in this application. First we investigate the coupling types (a) and (b). Then the influence of the subsystem's computational sequence is studied (for type (b) only).

(a) Source coupling. Here the two subsystems in (5.2) are coupled via algebraic variables $\mathbf{z}_\star$ in the algebraic equations $\mathbf{g}_\star$. Independent of the sequence of the subsystems in a dynamic iteration scheme, i.e., circuit-first or device-first, we always observe a dependence of the algebraic equation (iteration k) on old algebraic variables $(k-1)$. This holds true for Jacobi-iteration as well as a Gauss–Seidel approach. For the device-first approach, the Gauss–Seidel scheme reads as

$$\mathbf{F} := \begin{bmatrix} \mathbf{f}_d(\mathbf{y}_d^{(k)}, \mathbf{z}_d^{(k)}) \\ \mathbf{f}_c(\mathbf{y}_c^{(k)}, \mathbf{z}_c^{(k)}, \mathbf{z}_d^{(k)}) \end{bmatrix} \quad \text{and} \quad \mathbf{G} := \begin{bmatrix} \mathbf{g}_d(\mathbf{y}_d^{(k)}, \mathbf{z}_d^{(k)}, \mathbf{z}_c^{(k-1)}) \\ \mathbf{g}_c(\mathbf{y}_c^{(k)}, \mathbf{z}_c^{(k)}, \mathbf{z}_d^{(k)}) \end{bmatrix}, \tag{5.4}$$

where the superscript (k) denotes the iteration number. Since $\mathbf{G}$ depends on an old algebraic iterate, the contraction factor α_n does not vanish; see (3.7). Thus

convergence cannot be guaranteed by the structural analysis. The parameters of device and circuit will have a significant influence. This is discussed for a numerical example in section 5.5.

(b) Coupling with capacitance. Here, in system (5.3), the capacitance C_D is parallel to the device. The coupling of the two subsystems in the algebraic equations happens only in terms of differential variables; i.e., $\mathbf{g}_d$ depends on $\mathbf{y}_c$. According to Corollary 3.5 and Remark 3.4, convergence of the dynamic iteration is guaranteed for time windows size H small enough. Independent of the sequence of the subsystems, we will observe a dynamic iteration with convergence rate $\mathcal{O}(\sqrt{H})$ for $H \to 0$ for a Jacobi iteration approach.

According to Corollary 3.5, for the Gauss–Seidel approach we expect convergence rate $\mathcal{O}(H)$ if we start the iteration scheme by computing the circuit-subsystem first, since in this case the algebraic functions do not depend on old differential variables. If we exchange the sequence of the subsystems, i.e., start the iteration by computing the device subsystem first, and use the Gauss–Seidel approach, according to Remark 3.4 we only can guarantee convergence rate $\mathcal{O}(\sqrt{H})$.

However, the structure considered in the theory stated above is rather general, and our two subsystems exhibit less dependencies than the general case. Thus, we briefly address the two cases of Gauss–Seidel iteration for the system (5.3), i.e., circuit-first and device-first with the technique used above, in order to get a more detailed statement about the convergence rate of the fixed point iteration (3.7) in semiconductor-circuit coupled applications.

5.4. Analysis of the sequence of the subsystems. In this section, we address case (b) only, i.e., system (5.3), and assume that its two subsystems are of index 1. Then the functions $\mathbf{g}_c, \mathbf{g}_d$ are uniquely solvable with respect to $\mathbf{z}_c$ and $\mathbf{z}_d$, respectively. We furthermore assume the functions $\mathbf{f}_c$ and $\mathbf{f}_d$ to be Lipschitz-continuous in $\mathcal{U}_{d_0,n}$ (see also Assumption 3.1) with respect to all its components. Additionally, the implicit functions Φ_c and Φ_d determining $\mathbf{z}_c$ and $\mathbf{z}_d$ shall be Lipschitz-continuous.

DEFINITION 5.1 (Lipschitz constants). *We define the following abbreviations:*
L: Maximum of the Lipschitz constants of $\mathbf{f}_\star$ and $\Phi_\star$ w.r.t. $\mathbf{y}_\star$ and $\mathbf{z}_\star$ for $\star \in \{d, c\}$.
L_c: Maximum of L and the Lipschitz constant of $\mathbf{f}_c$ w.r.t. $\mathbf{z}_d$.
L_d: Maximum of L and the Lipschitz constant of Φ_d w.r.t. $\mathbf{y}_c$.

We note that the Lipschitz constants L_d and L_c can be regarded as the measure for the strength of the coupling between the two subsystems with respect to differential and algebraic variables, respectively.

LEMMA 5.2 (circuit-device error recursions). (i) *For the Gauss–Seidel scheme applied to* (5.3) *with device-first, the error recursion according to* (3.6) *reads as*

$$\begin{pmatrix} \delta_{\mathbf{y}}^k \\ \delta_{\mathbf{z}}^k \end{pmatrix} \le \underbrace{\begin{pmatrix} C_d H & 0 \\ C & 0 \end{pmatrix}}_{=:\mathbf{K_D}} \begin{pmatrix} \delta_{\mathbf{y}}^{k-1} \\ \delta_{\mathbf{z}}^{k-1} \end{pmatrix} + \begin{pmatrix} 1 + CH \\ C \end{pmatrix} |\Delta_{\mathbf{y}}^{k-1}(t_n)|. \tag{5.5}$$

(ii) *The circuit-first Gauss–Seidel scheme applied to* (5.3) *yields the error recursion*

$$\begin{pmatrix} \delta_{\mathbf{y}}^k \\ \delta_{\mathbf{z}}^k \end{pmatrix} \le \underbrace{\begin{pmatrix} 0 & CH \\ 0 & C_c H \end{pmatrix}}_{=:\mathbf{K_C}} \begin{pmatrix} \delta_{\mathbf{y}}^{k-1} \\ \delta_{\mathbf{z}}^{k-1} \end{pmatrix} + \begin{pmatrix} 1 + CH \\ C \end{pmatrix} |\Delta_{\mathbf{y}}^{k-1}(t_n)|. \tag{5.6}$$

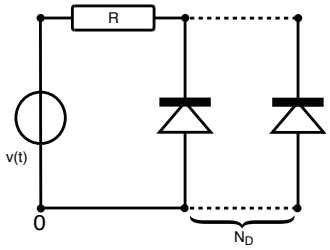

(a) Example circuit

Parameter	Physical meaning
$q = 1.6 \cdot 10^{-19}$ As	elementary charge
$\epsilon_s = 10^{-10}$ As/Vm	permittivity constant
$U_T = 0.026$ V	thermal voltage at $T_L = 300K$
$\mu_n/\mu_p = 0.15/0.045\,\mathrm{m}^2/\mathrm{Vs}$	low-field carrier mobilities
$C_0 = 10^{23}\,\mathrm{m}^{-3}$	maximum doping concentration
$l = 10^{-7}$ m	length
$A = 10^{-14}\,\mathrm{m}^2$	cross-section

(b) Physical parameters for a silicon *pn*-junction diode.

FIGURE 5.2. *Circuit and device parameters.*

Thereby it holds that

$$C_d = \frac{L_c L_d}{1 - L(1 + L_c)H_0}, \qquad C_c = \frac{L_c L_d}{1 - L(1 + L_d)H_0}, \tag{5.7}$$

with the maximum time window size H_0 and a suitable constant $C > 0$.

Proof. The fixed point iterations (i) and (ii) are in fact scalar equations for $\delta_{\mathbf{y}}^k$ and $\delta_{\mathbf{z}}^k$, respectively. Nonetheless this lemma can be proven analogously to Lemma 3.2. The only difference is that we distinguish between the Lipschitz constants here. ∎

THEOREM 5.3. *For the coupled semiconductor-circuit system with capacitance coupling* (5.3) *using a Gauss–Seidel dynamic iteration, the fixed point iteration is convergent with convergence rate $\mathcal{O}(H)$ for $H \to 0$. This holds independently of the computational sequence and on each time window. The leading order coefficients can be estimated by the constants C_d and C_c, given in* (5.7).

Proof. Convergence follows immediately from Corollary 3.5. The spectral radius of the iteration matrix $\mathbf{K_D}$ is given by $\rho(\mathbf{K_D}) = C_d H$. Thus we expect the convergence rate $C_d H$ for the device-first approach. Analogously the spectral radius of the iteration matrix $\mathbf{K_C}$ in (5.6) is given by $\rho(\mathbf{K_C}) = C_c H$, and thus we expect the convergence rate $C_c H$ for the circuit-first approach. ∎

Remark 5.4. Due to the special structure of our coupled semiconductor-circuit problem, we obtain convergence rate $\mathcal{O}(H)$ for the device-first approach, even if we observe a dependency of the algebraic constraints on old differential variables.

The speed of convergence of the dynamic iteration scheme depends on the leading order coefficients C_c and C_d. Thus it strongly depends on the constants L_c and L_d, which reflect the strength of the coupling via differential and algebraic variables and equations, respectively. The symmetry of C_c and C_d with respect to L_c and L_d can be observed in (5.7). Obviously, the device-first approach has a slower convergence for large L_c. This reflects a strong dependence of the circuit equations on the device model. Conversely, we get an increasing constant C_c for the circuit-first approach for large L_d. Below, this behavior will be verified by simulations.

5.5. Numerical results. We visualize the above results by the simulation of a series connection of a voltage source, a resistor, and a block of several (1D-modeled) silicon *pn*-diodes connected in parallel; see Figure 5.2(a). The circuit parameters are resistance $R = 1\Omega$ and the voltage source $v(t) = \sin(\omega t)$V with $\omega = 2\pi 10^{11}$ Hz. Each diode consists of a 50 nm n-region doped with C_0 and a 50 nm p-region doped with $-C_0$. Further parameters of the diode are given in Figure 5.2(b).

First we assume that the diode-block consists of 1500 identical diodes in parallel. Due to the parallel connection, accurate results are obtained by calculating one diode only and multiplying the output current by the number of devices.

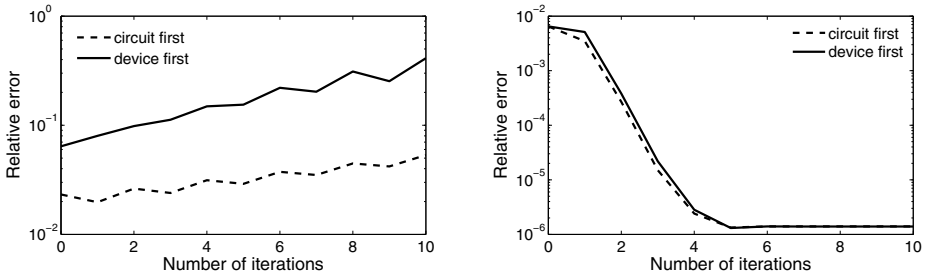

(a) Source coupling. (b) Coupling with capacitance.

FIGURE 5.3. *Relative error of network components between* 2.2–$2.3 \cdot 10^{-12} s$.

In the following simulations we applied an implicit Euler scheme with the constant time step size of $\Delta t = 0.1 \cdot 10^{-12}$s and simulated our circuit until $T = 10 \cdot 10^{-12}$s. The choice of the Euler scheme is merely due to the fact that we want to verify our analytic results unbiased by other effects. On each time window $H = \Delta t$ (i.e., each window is solved using exactly one step), we accomplish 10 iterations and compare the network variables computed with our dynamic iteration scheme below to a monolithic reference solution. The reference solution is made to verify the convergence of the iteration scheme to the solution of the monolithic systems. Therefore it is computed with the same step size but strongly coupled. For details of the algorithm we refer to [2].

(a) Source coupling. The iteration scheme for this coupling approach applied to the example circuit (Figure 5.2) does not converge. In Figure 5.3(a), we depict the relative error of the network components, i.e., the deviation from the reference solution, against the number of iterations in the time interval 2.2–$2.3 \cdot 10^{-12}$s. We choose this interval, since at this point the simulation breaks down. For both sequences—device-first or circuit-first—the iteration scheme clearly diverges. The different starting values for the two different sequences (Figure 5.3(a)) are due to bad convergence in the previous time windows and are the result of error propagation. We note that the amplification of the diode current by the factor of 1500 (due to the 1500 devices in parallel) causes the crucial parameter α in (3.7) to be greater than one, which results in divergence.

(b) Coupling with capacitance. Here we extract the capacitive behavior of each diode as a parallel capacitance $C_{\mathrm{D}} = 10^{-17}$ F. This results in an overall capacitance of $1.5 \cdot 10^{-14}$ F for the circuit subsystem. In turn, we compute the diode current $\mathbf{i}_{\mathrm{SD}}$ without displacement contribution. In contrast to the source coupling approach, we observe a convergent algorithm. In Figure 5.3(b) we depict the relative error (i.e., the relative deviation from the monolithic reference solution) of the network components against the number of iterations in the interval 2.2–$2.3 \cdot 10^{-12}$s, where the source coupling algorithm broke down. Clearly, we get convergence with the capacitance in parallel. Moreover, we observed significantly better convergence on the previous time windows.

We investigate the influence of the sequence of the subsystems on the speed of convergence of the dynamic iteration scheme. Therefore, we simulate the circuit given above for different numbers of parallel diodes, namely $N_D = 10$, 100, and 1000 devices. The number of devices is reflected by the Lipschitz constant L_c; i.e., for increasing N_D the Lipschitz constant L_c is increasing.

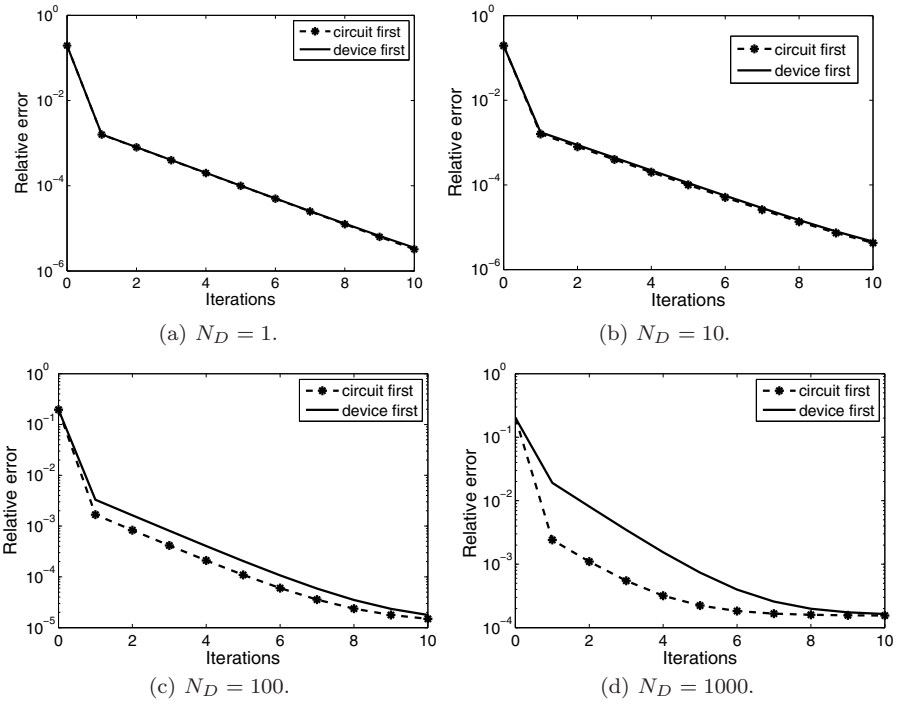

(a) $N_D = 1$. (b) $N_D = 10$.

(c) $N_D = 100$. (d) $N_D = 1000$.

FIGURE 5.4. *Relative error between* 0.4–$0.5 \cdot 10^{-12}s$ *for different numbers of diodes* N_D.

In Figure 5.4 we depict the convergence of the dynamic iteration scheme on one time window (we have chosen time window number 5) against the reference solution computed for respective number of diodes. Again, we used a time step size $\Delta t = 0.1 \cdot 10^{-12}$s. For the monolithic reference solution we applied the same step size. Figure 5.4 shows that for few diodes the speed of convergence is almost the same for both approaches. However, for more diodes the speed of convergence of the circuit-first approach becomes faster. For $N_D = 1000$ diodes we seem to save two iterations by using the circuit-first approach. Those results reflect the leading order coefficients C_d and C_c given in (5.7).

We note that for the increasing value of L_d we expect the device-first approach to be superior. This shows the importance of a proper estimation of the strength of the coupling, i.e., a proper estimation of the Lipschitz constants L_c, L_d, since by the value of those constants we can determine the optimal sequence for solving the subsystems.

Finally, we investigate the rate of convergence for our coupled simulation. To this end, we simulate the above introduced system for $2 \cdot 10^{-12}$s with capacitance coupling using either circuit-first or device-first approach. We apply only one Gauss–Seidel iteration per time window (i.e. $k_n = 1$). For time integration we use the first order implicit Euler method. According to the theory, we expect convergence rate $\mathcal{O}(H)$ (for window size $H \to 0$) already after one iteration of the dynamic iteration scheme on one window, for both approaches.

Figure 5.5 shows that both approaches yield a convergence rate in the order of the time window size H. Additionally, we see that for the larger Lipschitz constants L_c the circuit-first approach performs slightly better, as expected from Theorem 5.3.

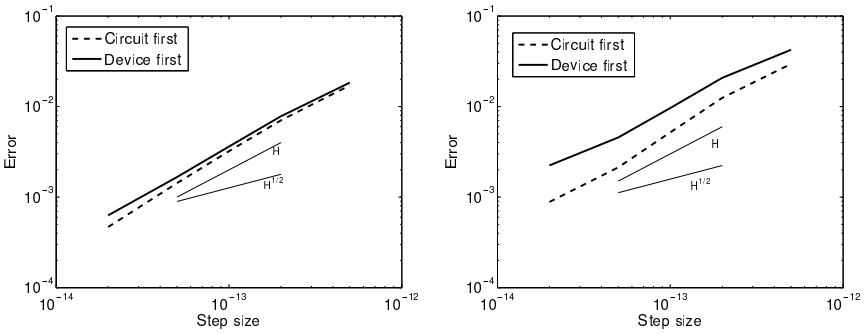

(a) $N_D = 100$. (b) $N_D = 1000$.

FIGURE 5.5. *Splitting error for different values of L_c after $2 \cdot 10^{-12}s$ for different time window sizes and for the circuit-first and device-first approach with one iteration per time window.*

6. Magnetostatic coupling. In a second application we consider the simulation of magnetic fields. Coupling of electric networks with distributed models of electrical energy transducers, e.g., transformers, is especially important if we seek to optimize and analyze the device's geometry, nonlinearity, etc. [28].

For low frequencies the electric displacement currents and the resistive eddy currents can be neglected in comparison to the currents induced by the magnetic field. This yields the *magnetostatic* approximation of Maxwell's equations. We will use dynamic iteration for coupled magnetostatic devices and electric circuits. Thereby we fit a lumped compact model (inductor) for the behavior of the magnetostatic PDE model of a transformer. This approach works analogously for other devices and applications (as we have seen in the semiconductor-circuit coupling), and it is shown to be highly efficient when multirate behavior is exploited [25]. After stating the coupled model, we examine its convergence properties.

6.1. Field device model. The transformer in our example circuit (Figure 6.1(a)) is described on a bounded 2D domain $\Omega \subset \mathbb{R}^2$ (Figure 6.1(b)). Its physical behavior is described by a magnetostatic model, which is discretized in space using Whitney elements; see [7]. Then the discretized device problem for the line-integrated magnetic vector potentials $\mathbf{a}$ reads as

$$\mathbf{K}_\nu(\mathbf{a})\mathbf{a} = \mathbf{X}_\mathrm{D}\mathbf{i}_\mathrm{D}, \tag{6.1}$$

which is equipped with circuit coupling equations, e.g., [24],

$$\frac{\mathrm{d}}{\mathrm{d}t}\mathbf{\Phi}_\mathrm{D} + \mathbf{R}_\mathrm{D}\mathbf{i}_\mathrm{D} = \mathbf{v}_\mathrm{D} \qquad \text{with} \qquad \mathbf{\Phi}_\mathrm{D} := \mathbf{X}_\mathrm{D}^\top\mathbf{a}. \tag{6.2}$$

Here $\mathbf{R}_\mathrm{D}$ denotes the device's DC resistances, $\mathbf{i}_\mathrm{D} = \mathbf{A}_\mathrm{D}\mathbf{i}$ and $\mathbf{v}_\mathrm{D} = \mathbf{A}_\mathrm{D}^\top\mathbf{v}$ are the currents and voltage drops of the coil windings, and $\mathbf{\Phi}_\mathrm{D}$ represents the magnetic flux. Each column of the matrix $\mathbf{X}_\mathrm{D}$ is a spatial discretization of a winding function, such that $\mathbf{X}_\mathrm{D}\mathbf{i}$ describes the spatial distribution of the applied currents $\mathbf{i}$. The curl-curl matrix $\mathbf{K}_\nu := \mathbf{C}^\top\mathbf{M}_\nu\mathbf{C}$ depends nonlinearly on the magnitude of the discrete flux density via the reluctivity to model saturation: $\mathbf{M}_\nu = \mathbf{M}_\nu(|\mathbf{C}\mathbf{a}|)$ with the discrete curl operator $\mathbf{C}$. Finally, the unknowns of the field system are $(\mathbf{a}, \mathbf{\Phi}_\mathrm{D}, \mathbf{i}_\mathrm{D})$. Note that in simulations $\mathbf{\Phi}_\mathrm{D}$ is not explicitly computed similar to flux-charged oriented MNA.

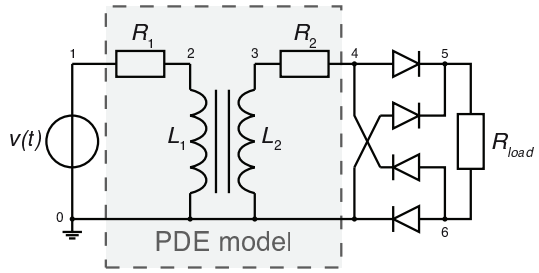

(a) Rectifier circuit, with four lumped diode models, winding and load resistance.

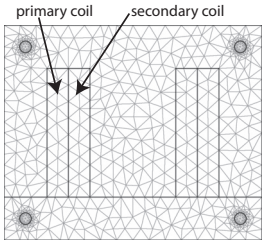

(b) Transformer PDE model, discretized by FEMM, [21].

FIGURE 6.1. *Nonlinear transformer embedded in nonlinear rectifier circuit.*

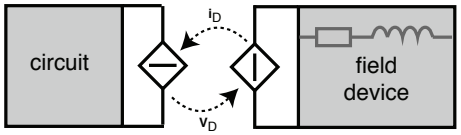

(a) Source coupling.

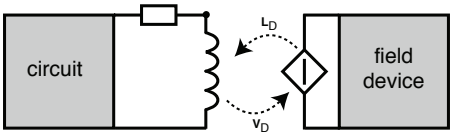

(b) Coupling with inductance.

FIGURE 6.2. *Coupling by current through the MQS device* (a) *and by an extracted inductance* (b).

For a known solution $\mathbf{a}^\star$ of (6.1), we can invert $\mathbf{K}_\nu(\mathbf{a}^\star)$, insert the result into the definition of $\mathbf{\Phi}_\mathrm{D}$, (6.2), and finally replace $\mathbf{\Phi}_\mathrm{D}$ in (6.2):

$$\frac{\mathrm{d}}{\mathrm{d}t}\big(\mathbf{L}_\mathrm{D}\mathbf{i}_\mathrm{D}\big) + \mathbf{R}_\mathrm{D}\mathbf{i}_\mathrm{D} = \mathbf{v}_\mathrm{D} \qquad \text{with} \qquad \mathbf{L}_\mathrm{D} := \mathbf{X}_\mathrm{D}^\top \mathbf{K}_\nu^{-1}(\mathbf{a}^\star)\mathbf{X}_\mathrm{D}. \tag{6.3}$$

This shows that (6.2) is the series connection of an inductor and a resistor.

6.2. Coupling. The structure of the model equations allows for two different representations and interpretations of the field-circuit coupling (see Figure 6.2):

(a) *source coupling*, in which the PDE model is represented in the circuit by a time-dependent current source $\mathbf{i}_\mathrm{D}$ (solving (6.2) for $\mathbf{i}_\mathrm{D}$), and conversely the circuit excites the PDE-model by a time-dependent voltage source,

(b) *coupling with inductance*, where the inductive effect (of the PDE) is described by a series connection of a resistor with constant resistance $\mathbf{R}_\mathrm{D}$ and a time-dependent inductor with inductance $\mathbf{L}_\mathrm{D}$ (6.3), and the PDE model is excited by a time-dependent voltage source.

In the parameter coupling (b), the inductance $\mathbf{L}_\mathrm{D}$ ($\mathbf{a}$) is fitted according to the solution $\mathbf{a}(t)$ of the discrete PDE problem (6.1).

In a monolithic simulation, the two field-circuit representations are equivalent: one can interpret (6.3) as the Schur complement of (6.1)–(6.2). But in a weak coupling by a dynamic iteration scheme, both approaches behave differently. The coupling with inductance uses more physical knowledge than the source coupling. But the drawback is the additional computational cost: the inductance matrices $\mathbf{L}_\mathrm{D}$ must be extracted by solving linear equations; cf. (6.3). For a given $\mathbf{v}_\mathrm{D}(t)$ the spatial discretization of the magnetostatic problem (6.1)–(6.2) yields an index-1 DAE. Additionally, we assume the coupled system to be of index-1 [5].

The abstract problem formulation is the same for source (a) and parameter coupling (b). Using the subscript c for the circuit and d for the Maxwell device,

we obtain

$$\begin{aligned} \dot{\mathbf{y}}_d &= \mathbf{f}_d(\mathbf{z}_d, \mathbf{z}_c), & \dot{\mathbf{y}}_c &= \mathbf{f}_c(\mathbf{y}_c, \mathbf{z}_c), \\ \mathbf{0} &= \mathbf{g}_d(\mathbf{y}_d, \mathbf{z}_d), & \mathbf{0} &= \mathbf{g}_c(\mathbf{y}_c, \mathbf{z}_c, \mathbf{z}_d), \end{aligned} \tag{6.4}$$

with nonsingular $\partial \mathbf{g}_d/\partial \mathbf{z}_d$ and $\partial \mathbf{g}_c/\partial \mathbf{z}_c$ (due to the index-1 assumption for the circuit). The differential variables of the circuit and field equations are $\mathbf{y}_c := (\mathbf{q}, \mathbf{\Phi})$ and $\mathbf{y}_d := \mathbf{\Phi}_{\mathrm{D}}$, whereas the corresponding algebraic unknowns are $\mathbf{z}_c := (\mathbf{u}, \mathbf{i}_{\mathrm{L}}, \mathbf{i}_{\mathrm{V}})$ and $\mathbf{z}_d := (\mathbf{a}, \mathbf{i}_{\mathrm{D}}, \mathbf{v}_{\mathrm{D}}, \mathbf{L}_{\mathrm{D}})$. Thus both coupling variables $\mathbf{i}_{\mathrm{D}}$ and $\mathbf{L}_{\mathrm{D}}$ are components of $\mathbf{z}_d$.

6.3. Dynamic iteration for the field-circuit system. Independent of the coupling type (a) or (b), a Gauss–Seidel-type (device-first) dynamic iteration for the field-circuit system reads as splitting functions:

$$\mathbf{F} := \begin{bmatrix} \mathbf{f}_d(\mathbf{z}_d^{(k)}, \mathbf{z}_c^{(k-1)}) \\ \mathbf{f}_c(\mathbf{y}_c^{(k)}, \mathbf{z}_c^{(k)}) \end{bmatrix} \quad \text{and} \quad \mathbf{G} := \begin{bmatrix} \mathbf{g}_d(\mathbf{y}_d^{(k)}, \mathbf{z}_d^{(k)}) \\ \mathbf{g}_c(\mathbf{y}_c^{(k)}, \mathbf{z}_c^{(k)}, \mathbf{z}_d^{(k)}) \end{bmatrix}. \tag{6.5}$$

The only old iterate $\mathbf{z}_c^{(k-1)}$, i.e., the voltage drop defined by the circuit, enters a differential equation via the function $\mathbf{f}_d$. This setting is similar to the semiconductor-circuit problem (coupling with capacitances); see Lemma 5.2. We do not repeat the proof here but conclude stability and convergence with rate $\mathcal{O}(\sqrt{H})$ by application of Corollary 3.5(i).

On the other hand it is not wise to reorder the computational sequence of the subproblems because a Jacobi or—as given here—the Gauss–Seidel approach with

$$\tilde{\mathbf{F}} := \begin{bmatrix} \mathbf{f}_d(\mathbf{z}_d^{(k)}, \mathbf{z}_c^{(k)}) \\ \mathbf{f}_c(\mathbf{y}_c^{(k)}, \mathbf{z}_c^{(k)}) \end{bmatrix} \quad \text{and} \quad \tilde{\mathbf{G}} := \begin{bmatrix} \mathbf{g}_d(\mathbf{y}_d^{(k)}, \mathbf{z}_d^{(k)}) \\ \mathbf{g}_c(\mathbf{y}_c^{(k)}, \mathbf{z}_c^{(k)}, \mathbf{z}_d^{(k-1)}) \end{bmatrix} \tag{6.6}$$

will exhibit a nonvanishing contraction factor α_n; see (3.7). Consequently, convergence is not guaranteed by the above theory, and divergence can occur similar to the semiconductor example shown in Figure 5.3(a). Moreover, even in the case of convergence, we can ensure only a convergence rate of $\alpha_n + \mathcal{O}(H)$.[1] Thus, in the following numerical investigation, we employ the sequence as given in (6.5).

6.4. Numerical results. In our application, the field model realizes a single-phase isolation transformer. Its configuration (see Figure 6.1(b)) is taken from the documentation of the software package `FEMM` (Finite Element Method Magnetics) [21]. The primary coil has 260 turns and the secondary coil has 90 turns. The reluctivity $\mathbf{M}_\nu$ is given by a highly nonlinear BH-curve taken from [11]. The attached rectifier circuit, Figure 6.1(a), is driven by a sinusoidal voltage source $v(t) = 160\sin(\omega t)\mathrm{V}$ with $\omega = 2\pi \cdot 60\mathrm{Hz}$. The diode currents are described by the lumped model

$$i = I_{\mathrm{s}} \cdot \left(\exp\left(\frac{v}{V_{\mathrm{th}}} \right) - 1 \right) + G \cdot v \quad \text{with} \quad G = 10^{-12} \frac{1}{\Omega}, \tag{6.7}$$

reverse saturation current $I_{\mathrm{s}} = 10^{-9}\mathrm{A}$, and thermal voltage $V_{\mathrm{th}} = 2.5 \cdot 10^{-2}\mathrm{V}$. The load resistor has a constant DC resistance of $R_{\mathrm{load}} = 10\Omega$. The resistances of the coil windings are extracted from the FEMM model. This gives $\mathbf{R}_{\mathrm{D}} = \mathrm{diag}(0.44937, 0.061526)\Omega$.

[1] In the parameter coupling case (b), the inductance enters the circuit effectively in a differential equation: the algebraic equation is just an evaluation; cf. (4.1b) vs. (4.1c). Thus the convergence guarantee can be extended to both sequences (device-first and circuit-first).

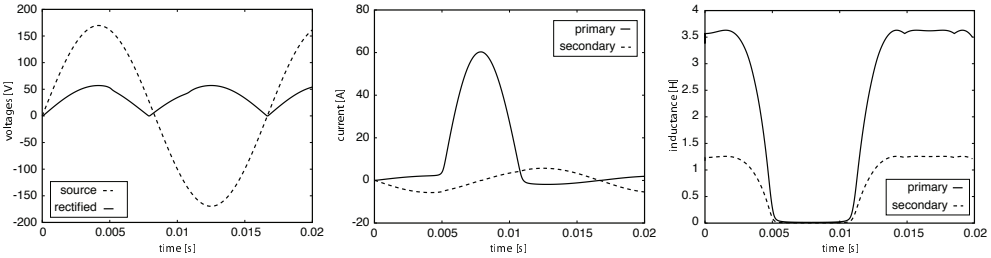

(a) Voltage drop at source (dashed line), and at the load resistance R_{load} (solid line).

(b) Currents through primary (solid) and secondary coil (dashed) of the transformer.

(c) Self-inductances of the primary (solid) and secondary coil (dashed) of the transformer.

FIGURE 6.3. *Voltages, currents, and inductance in the nonlinear transformer embedded in nonlinear rectifier circuit example, Figure* 6.1.

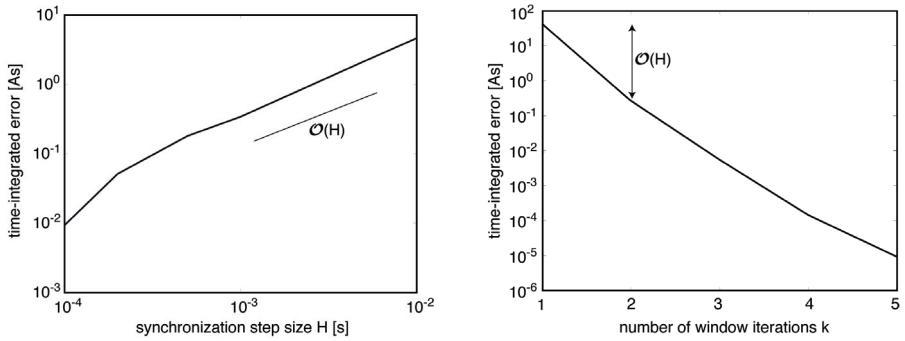

(a) The time-integrated error in the primary current on the full time interval in dependence of the synchronization step size H.

(b) Convergence of the primary current on the time window $[0,\ H]$ with $H = 5 \cdot 10^{-3}$ in dependence of the number of iterations.

FIGURE 6.4. *Convergence study of the dynamic iteration scheme applied to the field-circuit coupled problem using the time step size* $\Delta t = 10^{-5}$.

The problem is simulated on the time interval from $t_0 = 0$s until $t_e = 10^{-2}$s. For roughly a period of the applied signal, Figures 6.3(a)–(c) show voltages, currents, and inductances. The dynamics of the plots in Figures 6.3(b)–(c) are mainly due to the nonlinear saturation of the transformer; the current peak (primary coil) reflects the inrush current in this start-up phase of the transformer.

All time-integrations have been carried out by the implicit Euler method with a fixed time step size $\Delta t = 10^{-5}$s. We applied both the monolithic and the dynamic-iteration approaches to the problem in Figure 6.3. The monolithic simulation is used as a reference solution for the dynamic iteration approach. Thus we disregard the time-discretization error (introduced by Euler's method) and focus only on the splitting error of the iteration scheme (6.4). For a single-phase transformer, the extracted inductance $\mathbf{L}_{\text{D}}(t)$ corresponds to a 2×2 matrix for each time-step t. We use spline interpolation to recover a waveform from the discrete inductances. The dynamic iteration has been run for various window sizes $H = 5 \cdot 10^{-5}\text{s}, \ldots, 10^{-2}\text{s}$ and up to 5 iterations per window. Figure 6.4(a) shows the corresponding errors in the current through the first coil in dependence of those window sizes. We see—in accordance with the theoretic results of the previous section—that the error decreases with the time window size. In particular for small window sizes $H \approx \Delta t$ the first order accuracy

of the implicit Euler would dominate, and only higher order methods can yield an improvement here (independent of the number of window iterations).

The second convergence study, Figure 6.4(b), analyzes the number of iterations $k = 1, \ldots, 5$ per window. The plot shows the time-integrated error on the first time window $T = [0,\ H]$ with $H = 5 \cdot 10^{-3}$s for varying k. It matches the expected first order for a simple coupled problem: we have shown that there is no dependence on old iterates, and thus Corollary 3.5(ii) holds.

7. Conclusion. In this paper we have broadened the results of [3] and given a sufficient condition for the convergence of dynamic iteration schemes applied to general semi-explicit index-1 DAEs. The error propagation for the windowing technique was examined, and we have shown that under the given contractivity condition the dynamic iteration scheme is globally convergent and stable.

We have carried out a detailed analysis of important special cases of coupled index-1 problems. This included, e.g., the simple coupling, where for a Gauss–Seidel dynamic iteration scheme the rate of convergence with respect to the time window size H can be higher than in the general case, namely $\mathcal{O}(H)$ instead of $\mathcal{O}(\sqrt{H})$. Often optimal modeling of the coupling interface is necessary to obtain the higher convergence rate. In electrical engineering this can be of great interest since in applications incorporating radio frequency the chosen time window size usually is significantly smaller than one.

We have shown that the sequence in which different subsystems are simulated may be crucial to ensure convergence of the iteration scheme. Moreover, for the coupling of two subsystems we have shown that even if the contractivity condition is fulfilled for any sequence, the sequence of the subsystems influences the speed of convergence. As a measure of this we have identified the Lipschitz constants.

We have applied our theoretical results to two different applications in electrical engineering; a coupled semiconductor-circuit system and a coupled field-circuit system. For both applications we suggest a tailor-made modeling of the interface in order to ensure the best convergence of the applied iteration scheme. The simulations verify that our condition for convergence is sufficient. Moreover, the examples show that without enhanced modeling of the interface and thus without fulfilling the contractivity condition, the iteration may be divergent. Thus the examples not only verify the theoretical results, but also show that in DAE-PDE coupling iteration schemes can suffer from divergence—even for simple settings.

The identification of coupled systems consisting of more than two subsystems and coupling structures with a convergence rate higher than $\mathcal{O}(H)$ are subject to ongoing research. Furthermore, the consideration of the coupled field-semiconductor-circuit system is part of this ongoing research.

Acknowledgments. The authors especially thank Giuseppe Alì for the fruitful discussions and his suggestions for the initial proof of the fixed point iteration.

REFERENCES

[1] G. Alì, A. Bartel, and M. Günther, *Parabolic differential-algebraic models in electrical network design*, Multiscale Model. Simul., 4 (2005), pp. 813–838.

[2] G. Alì, G. Mascali, and R. Pulch, *Hyperbolic PDAEs for semiconductor devices coupled with circuits*, in Scientific Computing in Electrical Engineering SCEE 2008, J. Roos and L. R. J. Costa, eds., Math. Ind. 14, Springer, Berlin, 2010, pp. 305–312.

[3] M. Arnold and M. Günther, *Preconditioned dynamic iteration for coupled differential-algebraic systems*, BIT, 41 (2001), pp. 1–25.

[4] M. Arnold and A. Heckmann, *From multibody dynamics to multidisciplinary applications*, in Multibody Dynamics. Computational Methods and Applications, J. García Orden, J. Goicolea, and J. Cuadrado, eds., Springer, Berlin, 2007, pp. 273–294.
[5] A. Bartel, S. Baumanns, and S. Schöps, *Structural analysis of electrical circuits including magnetoquasistatic devices*, Appl. Numer. Math., 61 (2011), pp. 1257–1270.
[6] A. Bartel, *Partial Differential-Algebraic Models in Chip Design—Thermal and Semiconductor Problems*, Ph.D. thesis, Tehcnische Universität München, VDI Verlag, Düsseldorf, 2004.
[7] A. Bossavit, *Whitney forms: a class of finite elements for three-dimensional computations in electromagnetism*, IEE Proceedings, 135 (1988), pp. 493–500.
[8] M. Brunk and Kværnø, *Positivity preserving discretization of time dependent semiconductor drift–diffusion equations*, Appl. Numer. Math., 62 (2012), pp. 1289–1301.
[9] K. Burrage, *Parallel and Sequential Methods for Ordinary Differential Equations*, Oxford University Press, Oxford, UK, 1995.
[10] L. O. Chua and P. Y. Lin, *Computer Aided Analysis of Electronic Circuits*, Prentice-Hall, Englewood Cliffs, NJ, 1975.
[11] M. Clemens, S. Schöps, H. De Gersem, and A. Bartel, *Decomposition and regularization of nonlinear anisotropic curl-curl DAEs*, COMPEL, 30 (2011), pp. 1701–1714.
[12] F. Ebert, *On Partitioned Simulation of Electrical Circuits using Dynamic Iteration Methods*, Ph.D. thesis, Technische Universität, Berlin, 2008.
[13] D. Estévez Schwarz and C. Tischendorf, *Structural analysis of electric circuits and consequences for MNA*, Int. J. Circ. Theor. Appl., 28 (2000), pp. 131–162.
[14] U. Feldmann and M. Günther, *CAD-based electric-circuit modeling in industry I: mathematical structure and index of network equations*, Surveys Math. Indust., 8 (1999), pp. 97–129.
[15] K.-T. Grasser, *Mixed-Mode Device Simulation*, Ph.D. thesis, Technische Universität, Wien, 1999.
[16] E. Hairer, S. P. Nørsett, and G. Wanner, *Solving Ordinary Differential Equations* II: *Stiff and Differential-Algebraic Problems*, 2nd ed., Springer Ser. Comput. Math. Springer, Berlin, 2002.
[17] Z. Jackiewicz and M. Kwapisz, *Convergence of waveform relaxation methods for differential-algebraic systems*, SIAM J. Numer. Anal., 33 (1996), pp. 2303–2317.
[18] R. Kübler and W. Schiehlen, *Two methods of simulator coupling*, Math. Comput. Model. Dyn. Syst., 6 (2000), pp. 93–113.
[19] E. Lelarasmee, *The Waveform Relaxation Method for Time Domain Analysis of Large Scale Integrated Circuits: Theory and Applications*, Ph.D. thesis, University of California, Berkeley, 1982.
[20] L. D. Marini and P. Pietra, *New mixed finite element schemes for current continuity equations*, COMPEL, 9 (1990), pp. 257–268.
[21] D. Meeker, *Finite Element Method Magnetics User's Manual*, 2010. Version 4.2 (09Nov2010 Build).
[22] U. Miekkala and O. Nevanlinna, *Convergence of dynamic iteration methods for initial value problems*, SIAM J. Sci. Statist. Comput., 8 (1987), pp. 459–482.
[23] M. Rathinam and L. R. Petzold, *Dynamic iteration using reduced order models: A method for simulation of large scale modular systems*, SIAM J. Numer. Anal., 40 (2002), pp. 1446–1474.
[24] S. J. Salon, *Finite Element Analysis of Electrical Machines*, Kluwer, Dordrecht, The Netherlands, 1995.
[25] S. Schöps, H. De Gersem, and A. Bartel, *A cosimulation framework for multirate time-integration of field/circuit coupled problems*, IEEE Trans. Magn., 46 (2010), pp. 3233–3236.
[26] M. Selva Soto and C. Tischendorf, *Numerical analysis of DAEs from coupled circuit and semiconductor simulation*, Appl. Numer. Math., 53 (2005), pp. 471–488.
[27] R. Stratton, *Diffusion of hot and cold electrons in semiconductor barriers*, Phys. Rev., 126 (1962), pp. 2002–2014.
[28] I. A. Tsukerman, A. Konrad, G. Meunier, and J. C. Sabonnadière, *Coupled field-circuit problems: Trends and accomplishments*, IEEE Trans. Magn., 29 (1993), pp. 1701–1704.
[29] P. K. Vijalapura, J. Strain, and S. Govindjee, *Fractional step methods for index-1 differential-algebraic equations*, J. Comput. Phys., 203 (2005), pp. 305–320.
[30] J. K. White, F. Odeh, A. L. Sangiovanni-Vincentelli, and A. E. Ruehli, *Waveform Relaxation: Theory and Practice*, Tech. Report UCB/ERL M85/65, EECS Department, University of California, Berkley, 1985.